

CHAPTER 4

MEASURING THE STARK SHIFT OF THE $6S \rightarrow 7S$ TRANSITION

As discussed in Chapter 1, a test of the standard model using measurements of PNC in atomic cesium requires an accurate and precise calculation of atomic structure using atomic theory. The most objective way to test the accuracy of the theory is to compare its predictions with measurements of various atomic properties.

There are many measurements of the properties of cesium, including the lifetimes of the $6P$ states [40], and the hyperfine structure constants of the $6S$, $7S$ [41], $6P_{1/2}$, and $7P_{1/2}$ [42] states. All of these measurements agree with the predictions of Blundell *et al.* [14, 43, 44, 45] and Dzuba *et al.* [46, 15, 47, 48] to better than 1%. There was a notable exception to this good agreement in the measurement of the $6S \rightarrow 7S$ dc Stark shift, where the difference between the theory and the experiment [49] was 2%.

This chapter presents the theory of the dc Stark effect along with the details of our experiment that re-measures the dc Stark shift of the $6S \rightarrow 7S$ transition and eliminates the previous discrepancy. The details of the experiment include discussions of the requirement of a stable reference frequency and its implications for our data taking method and frequency stabilization schemes, the production and measurement of the electric field causing the Stark effect, and the determination of the dc Stark shift from our data. A presentation of our results concludes the chapter.

4.1 Theory of the dc Stark Effect

The theory of the dc Stark effect, which gives rise to the dc Stark shift, is discussed in detail in Ref. [50]. The full theory will not be repeated here. Instead, an outline of the calculation following that in Ref. [51] is presented. The interaction of an atom with a dc electric field \vec{E} can be described by the Hamiltonian

$$H_{\text{Stark}} = -e \sum_i \vec{r}_i \cdot \vec{E}, \quad (4.1)$$

where e is the electric charge, and \vec{r}_i is the vector from the nucleus to the i th electron. In Ref. [50] it is shown that this Hamiltonian can be broken into two components: $H_{\text{Stark}} = H_{\text{scalar}} + H_{\text{tensor}}$. The term H_{scalar} depends on only the magnitude of the electric field, while the term H_{tensor} depends on the field's direction as well as its magnitude.

The Stark Hamiltonian shifts energy levels as well as gives rise to the mixing discussed in Section 2.3.2, which permits the Stark-induced electric dipole transition. If the hyperfine structure is neglected, the energy shift is given by

$$\Delta\varepsilon(n, J, m_J) = -\frac{1}{2}\alpha_0 E^2 - \frac{1}{2}\alpha_2 \frac{3m_J^2 - J(J+1)}{J(2J-1)} \left(\frac{3E_z^2 - E^2}{2} \right), \quad (4.2)$$

where α_0 is the scalar polarization due to H_{scalar} and α_2 is the tensor polarization due to H_{tensor} . These two polarizations are given by

$$\alpha_0 = -\frac{2}{3} \sum_{n'J'} \frac{|\langle nJ | p | n'J' \rangle|^2}{(2J+1)(E_{nJ} - E_{n'J'})} \quad (4.3)$$

and

$$\alpha_2 = 2 \left[\frac{10J(2J-1)}{3(2J+3)(J+1)(2J+1)} \right]^{1/2} \times \sum_{n'J'} \frac{|\langle nJ | p | n'J' \rangle|^2}{E_{nJ} - E_{n'J'}} (-1)^{J+J'+1} \begin{Bmatrix} J & J' & 1 \\ 1 & 2 & J \end{Bmatrix}, \quad (4.4)$$

where E_{nJ} is the energy of the $|nJ\rangle$ state.

In this approximation it is clear that the tensor polarizability vanishes for $J = 1/2$. However, when higher orders of the theory are considered there is a contribution to α_2 from the combination of the off-diagonal matrix element of H_{tensor} between $J = 1/2$ and $J = 3/2$ states and the matrix element of the hyperfine structure operator between the same states. For the $L = 0$ states we are considering, this mechanism vanishes, but there are still tiny contributions due to the spin-dipolar part of the magnetic hyperfine structure and the quadrupole interaction [50]. In cesium, the tensor polarizability has been measured to be $\alpha_2 = -0.1372(79) \times 10^{-7} \text{ Hz}(\text{V}/\text{cm})^{-2}$ [52]. When compared with the scalar polarizability $\alpha_0 \sim 0.7 \text{ Hz}(\text{V}/\text{cm})^{-2}$ it is clear that the tensor polarizability is negligible. Therefore, we are only concerned with the scalar part of the dc Stark shift, which is independent of hyperfine level for energy shifts that are small compared to the fine structure splitting [53].

The energy shift due to the dc Stark shift of an $|nS_{1/2}\rangle$ state is given simply by

$$\Delta\varepsilon_{nS} = -\frac{1}{2}\alpha_{nS}E^2, \quad (4.5)$$

where α_{nS} is the scalar polarizability. The dc Stark shift of the $6S \rightarrow 7S$ transition is given by

$$\nu_{\text{Stark}} = -\frac{\alpha_{7S} - \alpha_{6S}}{4\pi}E^2 = kE^2. \quad (4.6)$$

To determine the constant k we scan across the $6S \rightarrow 7S$ transition at high and low electric fields, measure the line centers of the two scans, and calculate the frequency separation, $\Delta\nu_{\text{Stark}}$, of the two centers. Sample scans are shown in Fig. 4.1. The

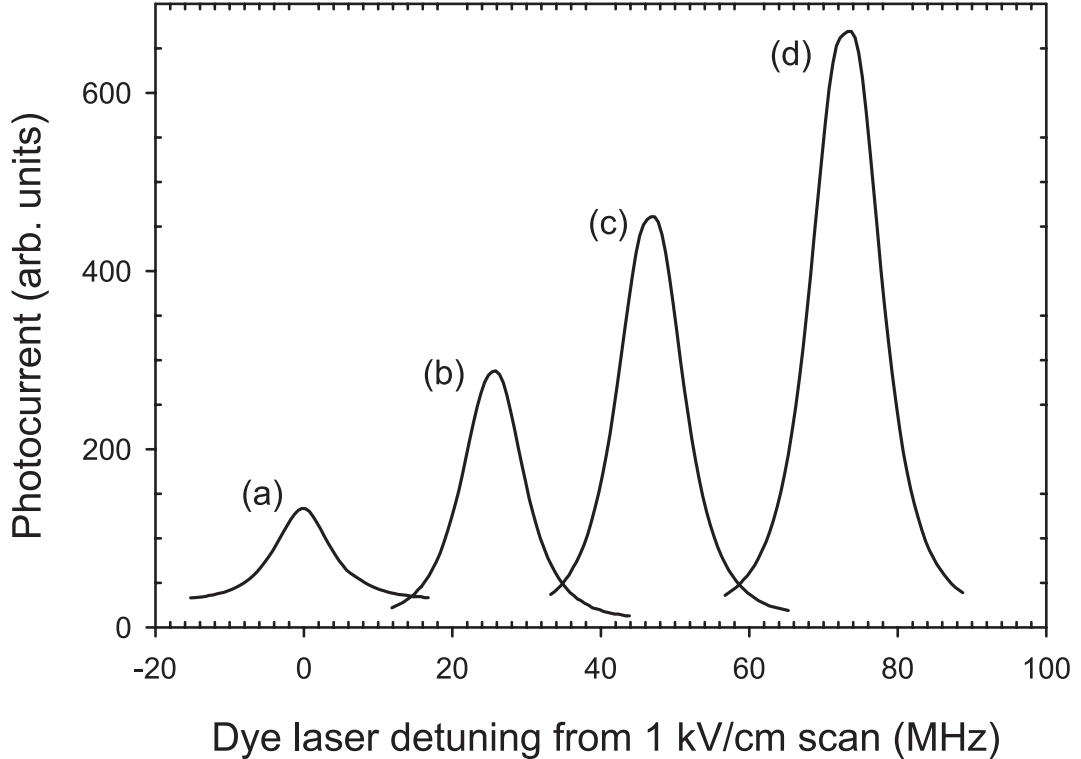


Figure 4.1: Four different scans of the $6S \rightarrow 7S$ transition with dc electric fields of (a) 1 kV/cm, (b) 6 kV/cm, (c) 8 kV/cm, and (d) 10 kV/cm.

value of k is then given by

$$k = \frac{\Delta\nu_{\text{Stark}}}{E_{\text{high}}^2 - E_{\text{low}}^2}. \quad (4.7)$$

Because the value of k is independent of hyperfine level, we use the transition with the highest signal-to-noise ratio: the $F = 3$ to $F' = 3$ transition.

4.2 Details of the Experiment

4.2.1 Data Scans and Frequency Drift

The major challenge in this experiment is determining the frequency separation of two scans to 0.1%. In order to make such a determination we must have a stable reference frequency. We use the reference cavity described in Section 3.3.5, which is the same cavity discussed in section 5.1.3 of Ref. [23]. In order to make

the cavity stable enough for the present experiment we have hermetically sealed the cavity and added a second stage of temperature stabilization. In addition, we use a simple peak locking scheme rather than the Pound-Drever-Hall locking scheme because of the latter's susceptibility to electronic offsets. The final frequency drift rate of the reference cavity averaged 0.5 MHz/min with a maximum observed drift of 0.8 MHz/min.

As described in Section 3.5, a computer controls the data acquisition. For this experiment the computer uses GPIB commands to control a Hewlett-Packard frequency synthesizer. The output from the synthesizer drives an acousto-optic modulator (AOM), which shifts the frequency of the dye laser light incident on the reference cavity. Since the dye laser is locked to the PBC, and the PBC is locked to the reference cavity, changing the AOM frequency causes the dye laser frequency to change by twice that amount. (Twice because the AOM is double passed. See the next section.)

The scans over the $6S \rightarrow 7S$ transition are 75 MHz wide and take approximately 8 seconds. The frequency separation between a scan at $E=1$ kV/cm and a scan at $E=10$ kV/cm is ~ 70 MHz. Therefore, the maximum allowable drift rate of the reference cavity is 0.5 MHz/min. Even smaller drift rates are required for lower electric fields. For all the data used in the final analysis we measured the drift before and after the measurement to ensure the rate was at an acceptable level.

4.2.2 Coupling Light into the Reference Cavity

The AOM is used to shift the frequency of the dye laser light incident on the reference cavity. Because the angle through which the light is diffracted by the AOM changes as the frequency of the AOM is changed, the AOM is “double-passed” as shown in Fig. 4.2. Double passing the light in the AOM works in the following way.

First we examine the horizontal motion by looking at the top view in

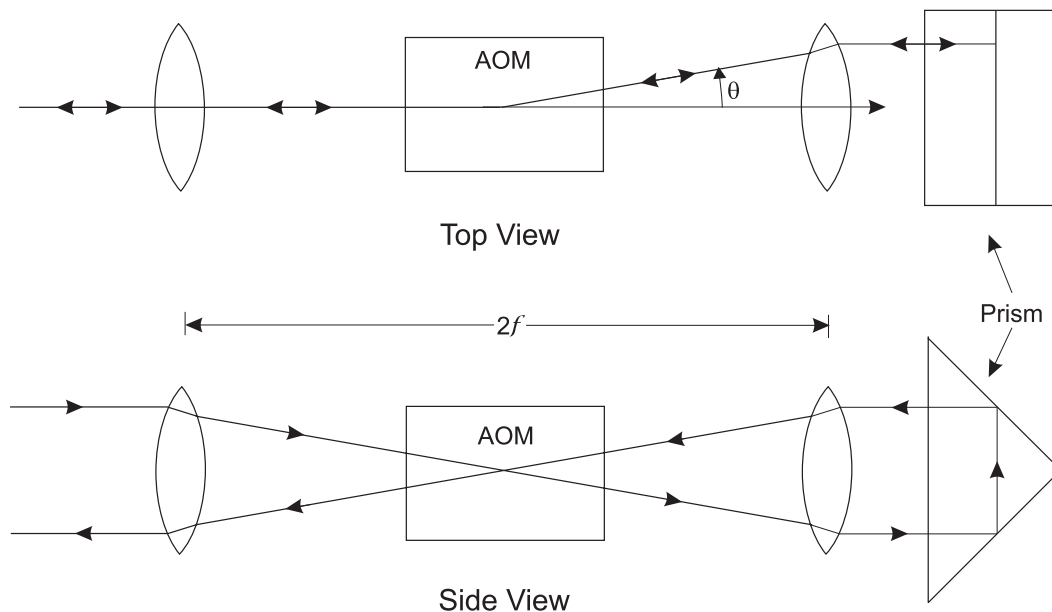


Figure 4.2: Top and side views of light “double-passed” through an AOM. Double passing the light eliminates most of the angular motion associated with a change in AOM frequency.

Fig. 4.2. The light to be passed through the AOM is centered horizontally on a lens that has a focal length f . The center of the AOM transducer is placed at the focal point of the lens, and the action of the AOM diffracts the light at some angle θ . The light then travels to another lens placed a distance f away from the AOM. This second lens also has a focal length f . The second lens bends the light back parallel to the initial direction of the laser beam. The beam is then retro-reflected off a prism and retraces its path back through the lenses and the AOM. As the frequency of the AOM changes, so does the angle θ . However, because of the positioning of the second lens, the laser beam is always normal to the prism and always gets retro-reflected. Therefore, the horizontal motion of the beam has been nearly eliminated.

A consequence of removing the horizontal motion of the laser beam is that the reflected beam travels back upon itself. This makes it difficult to use the light that has passed through the AOM. To describe the solution to this problem, we use

the side view in Fig. 4.2. The light incident on the lens-AOM system comes in above the center of the first lens. The first lens bends the light down through the AOM, causing the light to hit the second lens below its center. The second lens then brings the light back parallel to the initial direction and the prism reflects the light back with a vertical shift, and the light passes back through the second lens above its center. The second lens repeats the action of the first by bending the light down through the AOM and then low on the first lens. The beam is then bent back to parallel by the first lens. The result of the whole system is that the beam coming out of the lens-AOM system is lower than the one going in, but the horizontal motion does not change with changing AOM frequency. The lower beam is easily directed to the reference cavity.

The double-passed AOM system does not eliminate all the motion; the angular displacement with a change in frequency of ~ 40 MHz is ~ 0.3 mrad, compared with the usual 260 mrad. This is sufficient to keep the laser beam from moving off the reference cavity. It is not sufficient for measuring 70 MHz separations to 0.1%, however. The reason is as follows.

The reference cavity was constructed to be a confocal cavity. However, the limitations of experimental science preclude us from building a perfectly confocal cavity, so the cavity is only **nearly** confocal. As a result, adjacent modes are not perfectly degenerate. The transmission through the reference cavity of three such modes, (a), (b), and (c), into which the light might couple is shown in Fig. 4.3. As the light incident on the reference cavity moves, the coupling into each mode changes. Figure 4.4(d) shows the results when 60% of the light is coupled into mode (a), 30% is coupled into mode (b), and 10% is coupled into mode (c). Figure 4.4(e) shows the results when the fractions coupled into mode (a) and mode (c) are reversed. Because we use a locking scheme that locks the laser frequency to the frequency of the maximum transmission of the reference cavity, the lock point of the laser frequency will change as the coupling changes. To eliminate this problem from beam

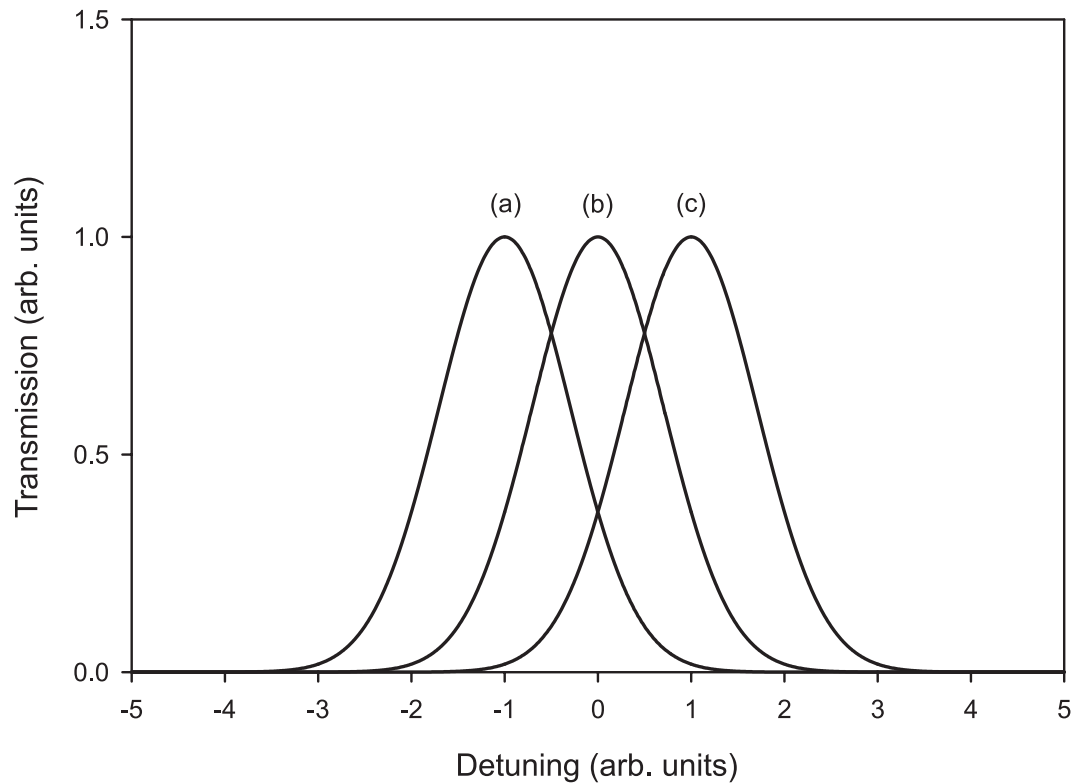


Figure 4.3: Transmission versus frequency of three nearly degenerate modes of the reference cavity.

motion on the reference cavity, we couple the light from the double-passed AOM into one end of a 0.3 m length of single mode optical fiber. The other end of the fiber is fixed to an optical mount. By using this scheme, the **intensity** of the light incident on the reference cavity changes by up to 20% because the light from the AOM moves on the face of the fiber, which changes the coupling efficiency into the fiber. However, the output end of the fiber remains fixed, and thus the light into the reference cavity remains motionless. The variations in intensity transmitted through the fiber do not affect the lock point of the dye laser.

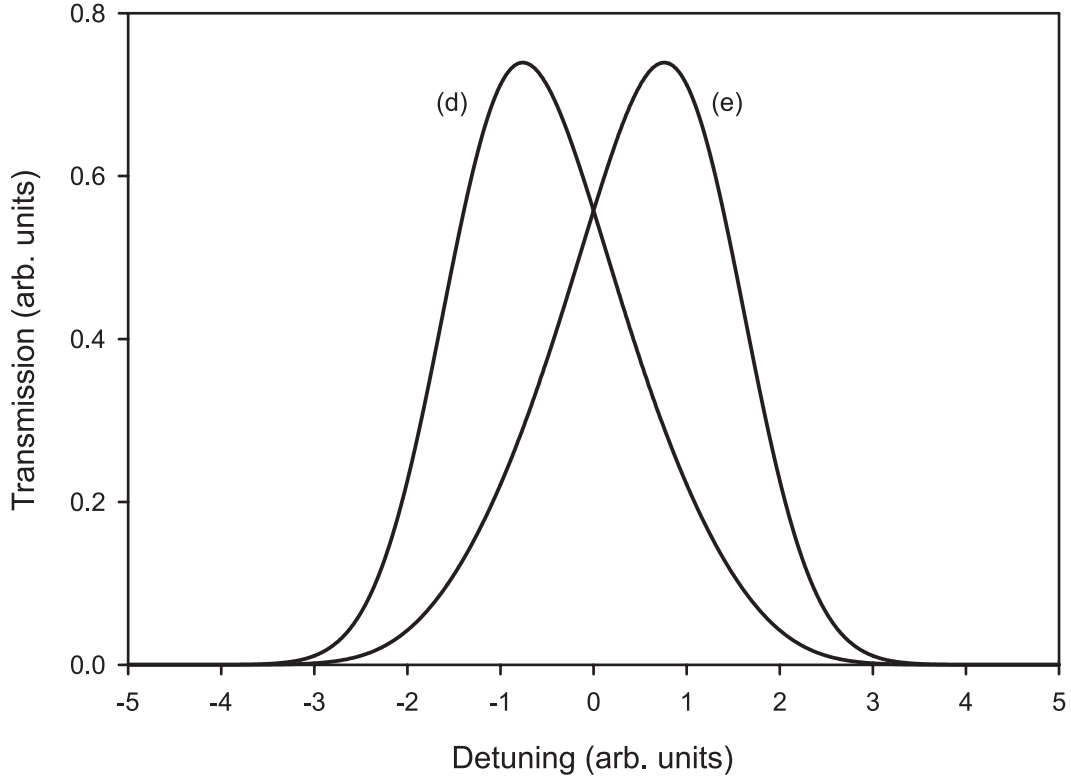


Figure 4.4: Total transmission through the reference cavity versus frequency. The transmission when 60% of the light is coupled into mode (a) (from Fig. 4.3), 30% of the light is coupled into mode (b), and 10% of the light is coupled into mode (c). The transmission shown in (e) is when the fraction of light coupled into modes (a) and (c) has been reversed.

4.2.3 Production and Measurement of the Electric Field

The electric field plates used in this experiment are different from those used in the PNC measurement and in the measurement of β . The plates are $2 \times 5 \times 0.5$ cm blocks of molybdenum mounted in a plexiglas bracket. The plates are separated by 0.48994(25) cm. They were made smaller than the plates used in the PNC experiment to keep them as far away from other conducting surfaces as possible in order to handle safely the 5 kV applied across the plates. In addition, all the corners and sharp edges on the plates are rounded or smoothed to prevent arcing.

The voltage on the plates is measured with a high-voltage probe that was

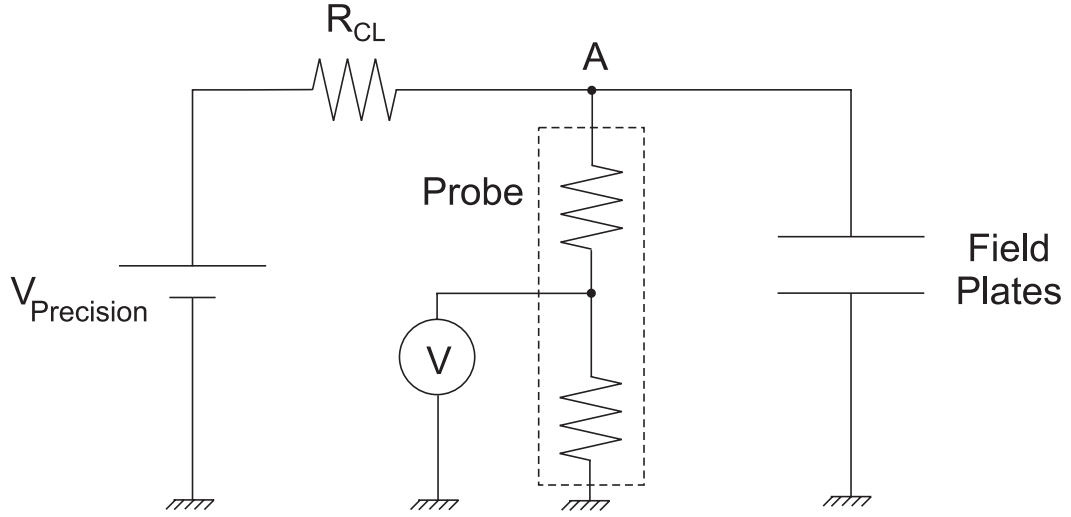


Figure 4.5: The voltage divider measurement of E at point A for the dc Stark shift measurement. $V_{\text{precision}}$ is the high-voltage source, R_{CL} is a current-limiting resistor, and the two resistors and the dashed box are the high-voltage probe. The experiment is always run with the probe in place because the probe and R_{CL} in series make a second voltage divider that changes the voltage at A.

calibrated with a NIST-traceable voltage source in the JILA electronics shop. The probe divides the voltage applied to the plates by 901.52(5). The method for measuring the voltage is shown in Fig. 4.5. It is important to note that when the high-voltage probe is in place it makes a voltage divider with the current-limiting resistor R_{CL} . This divider causes a voltage drop across R_{CL} . If the experiment is performed with the probe removed the voltage on the plates will be different than the voltage that was measured. Because of this difference, the probe is left connected at all times.

4.3 Determination of the dc Stark Shift

4.3.1 Determination of Line Centers

To obtain the transition rate versus frequency plots for this experiment, we lock the laser and the cavities with the AOM frequency set in the middle of its

range. We then change the voltage on the reference cavity piezo to tune the dye laser frequency to the peak of the $6S \rightarrow 7S$ transition*. The computer then quickly sweeps the voltage controlling the AOM frequency to a point below the $6S \rightarrow 7S$ transition and then sweeps the voltage across the transition in small steps, taking a 16.667 ms long data point at each step.

An accurate determination of the center of each scan is critical to the success of this measurement. Because the ac Stark effect can cause broadening of the line shape and large frequency shifts of its effective center [$\sim 21 \text{ MHz}/(\text{MW}/\text{cm}^2)$] [30] we keep the intensity inside the PBC as low as possible. The intensity in this experiment is 200 W compared with the intensity of 4 kW typical for the PNC experiment. Our intensity reduces the ac Stark shift to 0.84 MHz. This is much larger than the acceptable uncertainty on our measurement of high- and low- E peak separations. However, the ac Stark shift does not depend on the dc electric field. Therefore, this small ac Stark shift does not affect the accuracy of our measurement.

Because of the asymmetry introduced by the ac Stark shift, it is impossible to fit our line shapes to a simple function. Therefore it is not straight forward to determine the line center. The line shape does not change significantly with E , however, so it is possible to determine an **effective** line center for each scan. The “center” of a line is found by taking the two frequencies at which the probe signal is $n/10$ times its peak value and averaging the pair of frequencies for each $n = 1, 2, \dots, 9$. The effective center is then the average of these nine values. We test the reproducibility of this method by changing slightly the value of the probe signal at which we determine the two frequencies. For example, instead of taking the values at $n/10$, we can take the values at $1.01 \times n/10$. The reproducibility of finding line centers in this manner is 0.02 MHz.

We find that saturation of the $6S \rightarrow 7S$ transition can cause small shifts in

*Of course, we only adjust the reference cavity before the initial scan. For successive scans the cavity serves as the frequency reference.

the effective line center. Scans over the transition with and without saturation are shown in Fig. 4.6. As can be seen in Eq. (2.27), the $6S \rightarrow 7S$ “ α ” transition rate has two terms. To avoid an error from saturation we rotate the linear light until ϵ_x is roughly 10% smaller than its smallest value at which we can measure a shift of the line center. Therefore, there is no effect on our determinations of the line centers from saturation. The small β terms are larger as a result, but the relative size of the “ α ” rate to the “ β ” rate is $(\alpha/\beta)^2 = 98.1$, so the small β terms are still unimportant*. In the end we determine the line center to approximately 2 parts in 1000.

4.3.2 Determination of Frequency Separation of two Electric Fields

If the reference cavity were perfectly stable, determining the frequency separation between a low- E scan and a high- E scan would be trivial. However, the reference cavity has a nonzero drift rate as previously discussed. As can be seen in Fig. 4.7, the drift can be nonlinear, even reversing direction from time to time. Taking several scans at high and low electric fields in succession is sufficient to eliminate a linear drift. To account for the nonlinear drift we use a standard least squares technique [54] to fit the centers of 16 scans, which alternate between high and low E , to a third order polynomial plus a constant. The extracted constant is the dc Stark shift. Our final fractional uncertainty in $\Delta\nu_{\text{Stark}}$, which is dominated by the uncertainty in the determination of the line centers, is 0.04% for each ten scan set.

4.4 Results

Once we can determine the separation between two scans taken with different electric fields we can, in principle, determine the value of k . However, a more precise determination can be made if we extract k from the fit to data taken at

*Even if the “ β ” terms do become appreciable, their contribution to the line shape scales the same way the “ α ” contribution does. Therefore, the frequency shift between effective line centers will be the same as in the absence of the “ β ” transition.

several different values of the high field. Determinations of k from pairs of fields (eg. 1 kV/cm and 10 kV/cm) are shown in Fig. 4.8. The weighted average of the 14 scans is $0.72618(19)$ Hz (V/cm) $^{-2}$. The fit of the data to $\Delta\nu_{\text{Stark}} = kE^2$, along with a plot of the residuals is shown in Fig. 4.9. The slope of the line fitting the data is $k = 0.72620(13)$ Hz (V/cm) $^{-2}$. The reduced χ^2 's for the fit and the weighted average both indicate a 60% probability that the data are from a random distribution. The contributions to the uncertainty in our final result for k are 0.1% from the measurement of the field plate separation*, 0.04% from the determinations of $\Delta\nu_{\text{Stark}}$, and 0.01% from the measurement of the applied voltage. This yields a total fractional uncertainty of 0.11%. Our final result is

$$k = 0.7262(8) \text{ Hz(V/cm)}^{-2}, \quad (4.8)$$

which disagrees with the previous result of $0.7103(24)$ Hz (V/cm) $^{-2}$ [49], but is in excellent agreement with theoretical prediction $k = 0.7257$ Hz (V/cm) $^{-2}$ of Blundell *et al.* [14], and is within 0.3% of the prediction $k = 0.7237$ Hz (V/cm) $^{-2}$ of Dzuba *et al.* [55]. These data are shown in Fig. 4.10. The difference in polarizabilities of the two states, $\alpha_{7S} - \alpha_{6S}$ can be extracted from these numbers. In atomic units, our result is $\alpha_{7S} - \alpha_{6S} = 5837(6)$ compared with the predictions of Blundell *et al.* ($\alpha_{7S} - \alpha_{6S} = 5833$) and Dzuba *et al.* ($\alpha_{7S} - \alpha_{6S} = 5817$). We have attempted to determine the source of the disagreement between the present work and that of Watts *et al.* [49]. However, Watts, who carried out the primary data analysis, is deceased and the records of his analysis are no longer available.

*We measure the separation of the plates by using a high-precision height-micrometer and a dial indicator to measure the difference in each plate's height above a flat granite surface. A more precise measurement could be made optically, but the constraints of the experiment prevent us from constructing the plates out of materials that would allow such a measurement. (See Ref. [13], Section 5.2.)

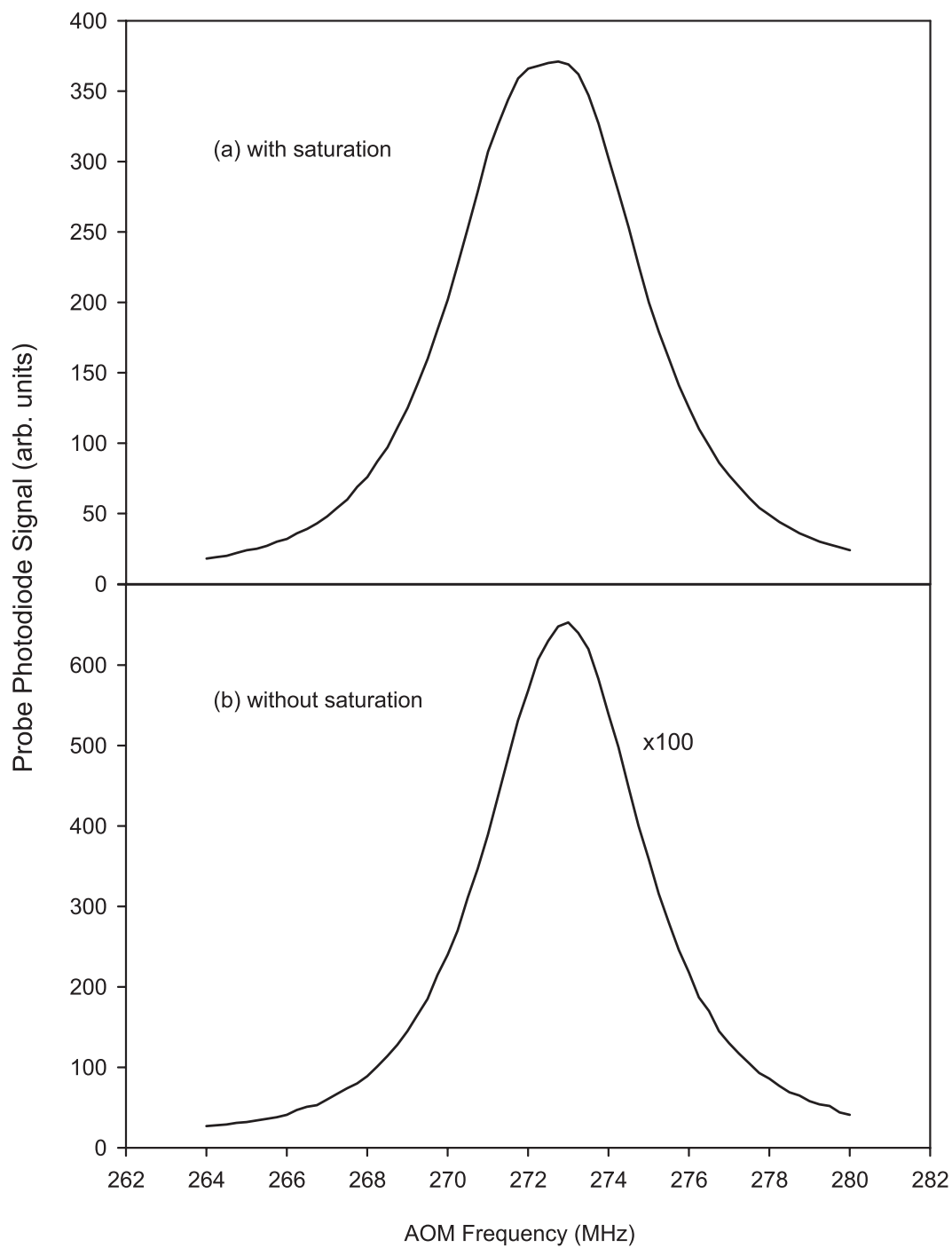


Figure 4.6: Scans over the $6S \rightarrow 7S$ transition (a) with and (b) without saturation. In (a) the electric field is 9 kV/cm and in (b) the electric field is 1 kV/cm. Note that in (b) the signal has been increased by a factor of 100.

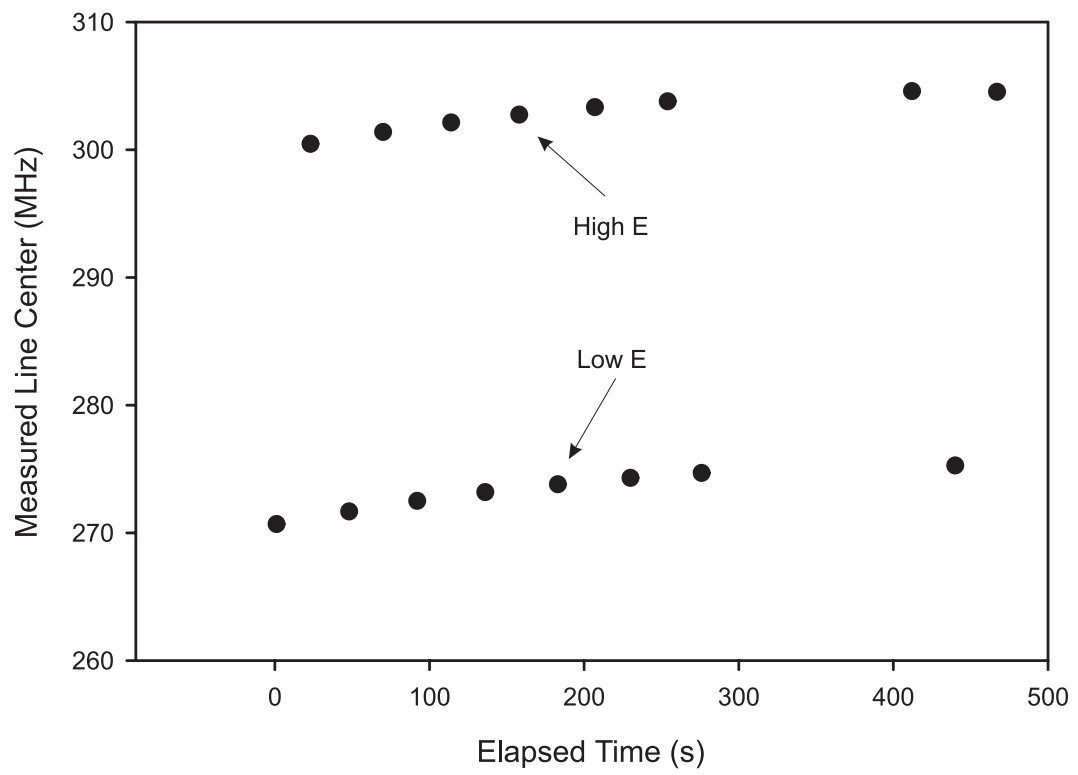


Figure 4.7: Typical data from a data “set” showing the drift of the reference cavity. The separation between the data points is the dc Stark shift.

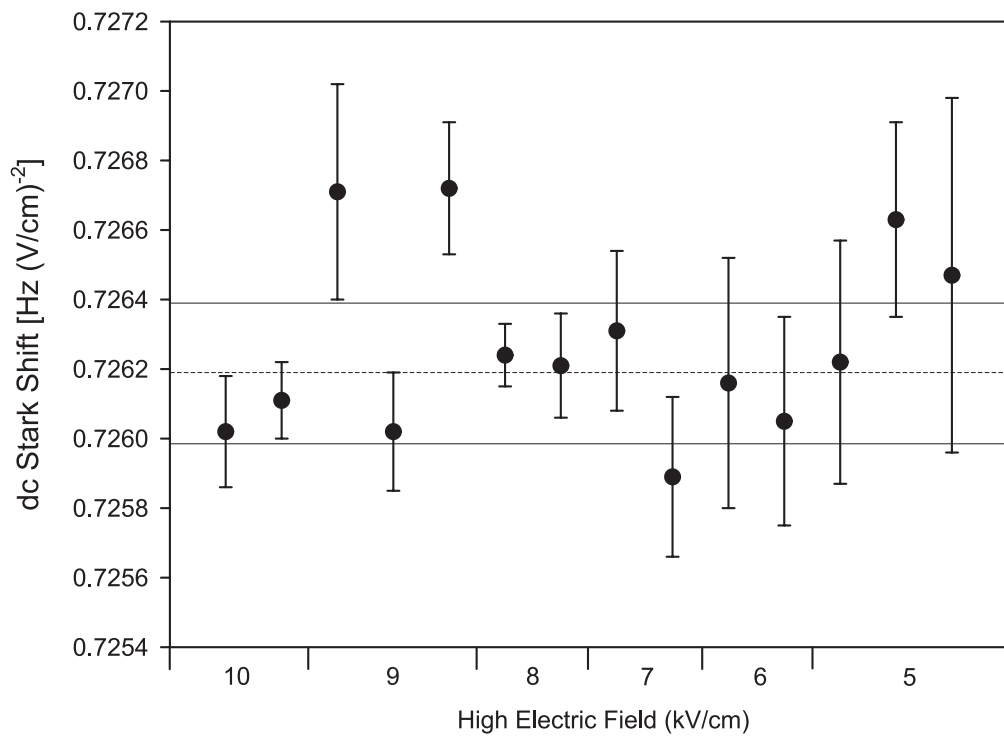


Figure 4.8: Determinations of k from pairs of electric fields. The high field value is shown on the \hat{x} axis. The dashed horizontal line is the weighted average $k = 0.72618(19) \text{ Hz (V/cm)}^{-2}$ and the solid lines show the one σ error bars.

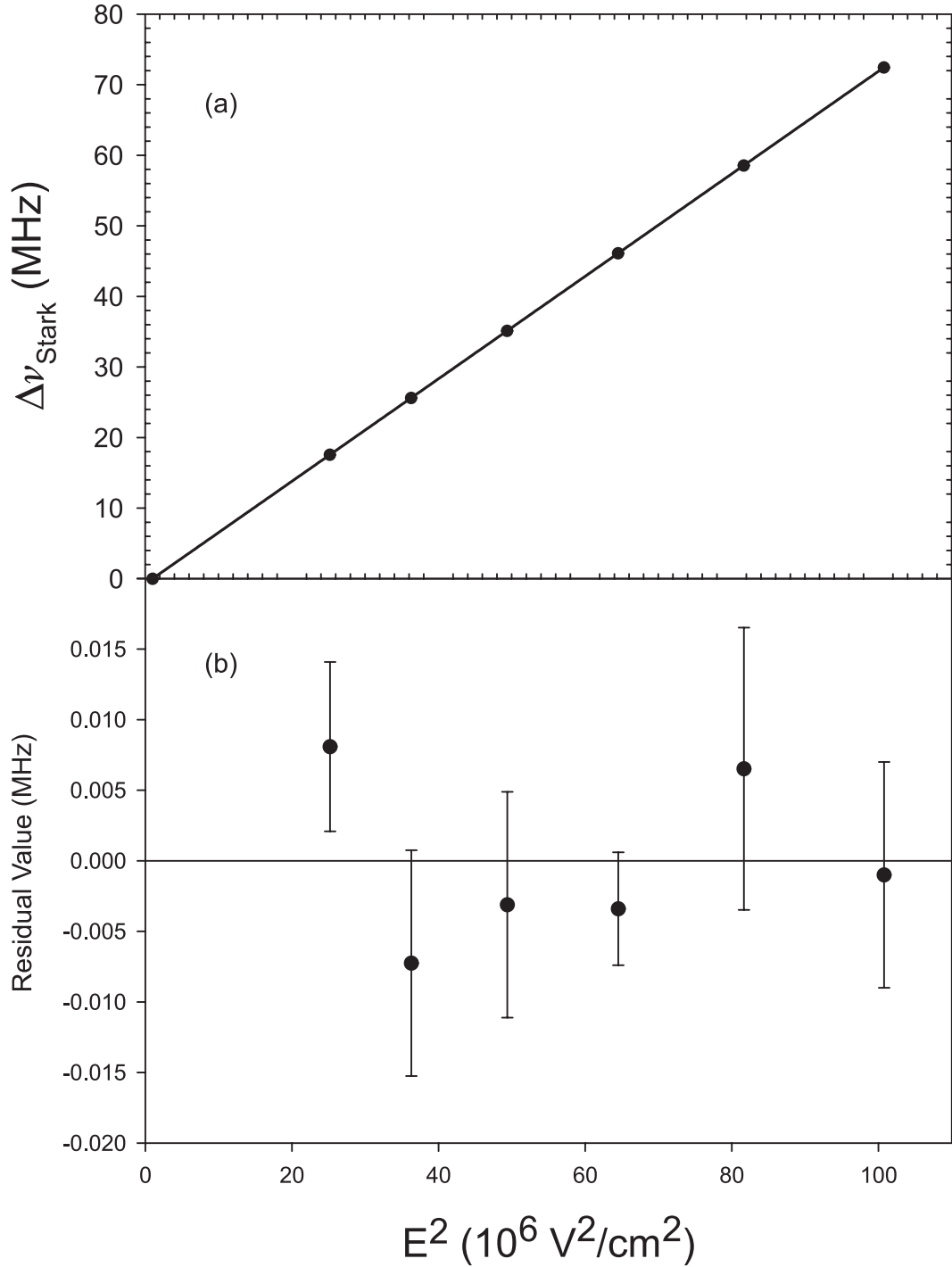


Figure 4.9: (a) Measured values and (b) residuals of $\Delta\nu_{\text{Stark}}$ plotted as a function of E^2 . In (a) The error bars are smaller than the data points and values from scans with the same values of E have been averaged together. The solid line is a fit to the data assuming $\Delta\nu_{\text{Stark}} \propto E^2$. The result is $k = 0.72620(13)$ Hz (V/cm) $^{-2}$.

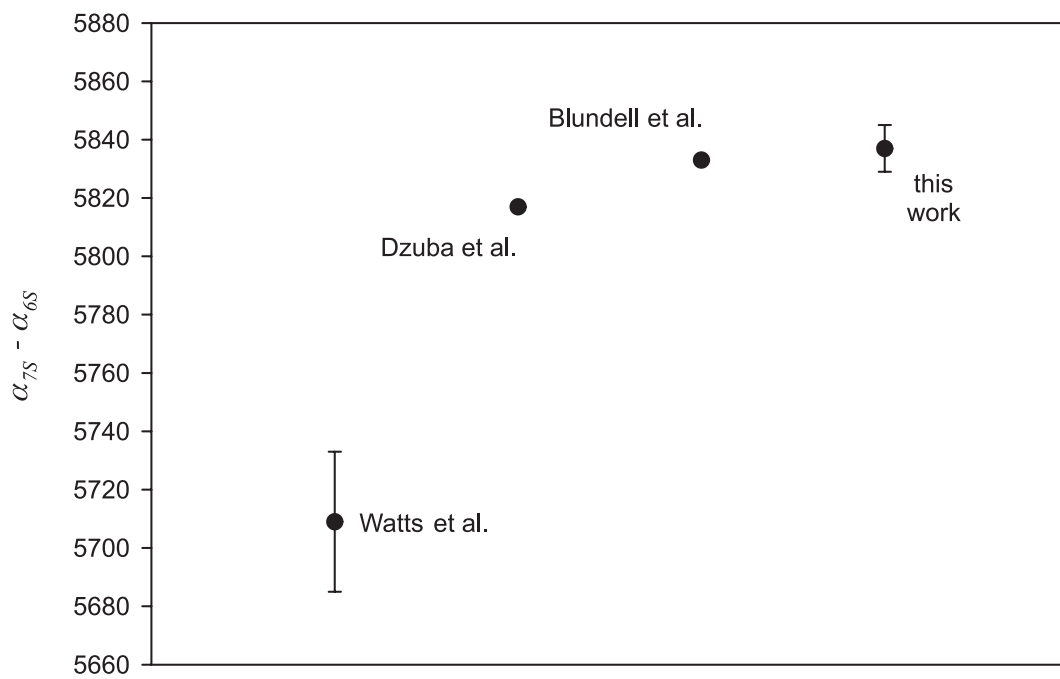


Figure 4.10: A comparison of determinations of the dc Stark shift of the $6S \rightarrow 7S$ transition. The number of Watts *et al.* is from Ref. [49], the number of Dzuba *et al.* is from a private communication, and the number of Blundell *et al.* is from Ref. [14].